International Journal of Neural Systems, Vol. 0, No. 0 (2020) 1–16

Incorporating Uncertainty in Data Labeling into Automatic Detection of Interictal Epileptiform Discharges from Concurrent Scalp EEG via Multi-way Analysis

Bahman Abdi-Sargezeh
School of Science and Technology, Nottingham Trent University, Nottingham, UK

Antonio Valentin
Department of Clinical Neuroscience, King's College London, UK

Gonzalo Alarcon
Department of Neurology, Hamad General Hospital, Doha, Qatar

Saeid Sanei*
School of Science and Technology, Nottingham Trent University, Nottingham, UK
E-mail: saeid.sanei@ntu.ac.uk

Interictal epileptiform discharges (IEDs) are elicited from an epileptic brain, whereas they can also be due to other neurological abnormalities. The diversity in their morphologies, their strengths, and their sources within the brain cause a great deal of uncertainty in their labeling by clinicians. The aim of this study is therefore to exploit and incorporate this uncertainty (the probability of the waveform being an IED) in the IED detection system which combines spatial component analysis (SCA) with the IED probabilities referred to as SCA-IEDP-based method. For comparison, we also propose and study SCA-based method in which probability of the waveform being an IED is ignored. The proposed models are employed to detect IEDs in two different classification approaches: (1) subject-dependent and (2) subject-independent classification approaches. The proposed methods are compared with two other state-of-the-art methods namely, time-frequency features and tensor factorization methods. The proposed SCA-IEDP model has achieved superior performance in comparison with the traditional SCA and other competing methods. It achieved 79.9% and 63.4% accuracy values in subject-dependent and subject-independent classification approaches, respectively. This shows that considering the IED probabilities in designing an IED detection system can boost its performance.

Keywords: EEG interictal epileptiform discharges; IED detection; IED morphology; labeling uncertainty; tensor decomposition.

1. Introduction

Epilepsy is a chronic brain disease characterized by epileptic seizures occurring due to excessive discharges of a group (or groups) of neurons in the cerebral cortex or hippocampus.[1] Some events, called interictal epileptiform discharges (IEDs), occur between two seizure onsets, which can be captured by electroencephalography (EEG).[2] The IEDs are often in the form of sharp spikes lasting for 20-70 ms or sharp waves lasting for 70-200 ms.[3]

Around 30% to 40% of patients requiring epilepsy surgery need invasive intracranial EEG (iEEG) recording[4] since the sensitivity of scalp-EEG is low for epilepsy diagnosis. A large proportion of IEDs are invisible in the scalp-EEG. Studies investigating iEEG and scalp-EEG simultaneously have shown that only a small percentage of IEDs (9% in Ref.[5] and 22% in Ref.[6]) can be seen in scalp-EEG by visual inspection. This may be owing to the relatively

high attenuation of electrical fields due to being away from the source.[7–9] Therefore, most studies use subdural recordings for detecting IEDs,[10,11] which gives higher accuracy as compared to scalp recordings. However, Koessler *et al.* have demonstrated that the IED signatures are contained in the scalp-EEG regardless of IEDs deep locations.[12] These signatures can be partial spikes or the likelihood of scalp IEDs and can be captured via multi-way analysis. The purpose of the paper is to detect IEDs from the scalp, and in particular, those discharges not identifiable on the scalp by simple visual inspection.

In places where only the scalp-EEG is recorded and analyzed,[13,14] the scalp-invisible IEDs are not considered. Therefore, studying simultaneous iEEG and scalp-EEG recordings and designing an algorithm to detect the scalp-invisible IEDs from scalp-EEG are of great interest. The foramen ovale (FO) electrodes[15] provide an opportunity to simultaneously record scalp-EEG and iEEG without disruption to brain coverings.[16,17] They are less invasive compared to depth electrodes and bilaterally introduced via infra-orbital foramen into ambient cistern adjacent to the mesial temporal lobe where the source of mesial temporal lobe epilepsy is.[16,18]

Models provided for detection of IEDs scored by scalp-EEG are inadequate since they are unable to detect the scalp-invisible IEDs, thereby being biased to detect only a subset of IEDs which are visible over the scalp. Only very few studies have been carried out to investigate scalp IEDs from simultaneous scalp-EEG and iEEG recordings.[19–21] Spyrou *et al.*[19] detected scalp-visible and scalp-invisible IEDs, scored by iEEG, from scalp-EEG by using time-domain, wavelet transform, chirplet transform, and time-frequency features. Others[20] mapped scalp-EEG to iEEG by proposing an asymmetric–symmetric autoencoder, then detected the IEDs by using a convolutional neural network.

Tensor factorization and multiview classification have recently attracted the attention of researchers in biomedical signal processing.[22,23] Several electrodes may capture the IED signatures due to originating IEDs from the temporal brain region around the same time, meaning that the EEG channels are spatially and temporally correlated. Therefore, multichannel and multi-trial (multi-segment) EEG processing using tensor decomposition methods is expected to be effective in IED detection. Spyrou *et al.* developed a model based on Tucker decomposition for IED detection from concurrent scalp-EEG and iEEG recordings.[21] In a recent approach,[24] nonnegative Tucker decomposition (NTD) was used for epileptic spike detection from scalp-EEG.

The IEDs have a wide variety of morphologies. They may appear as a sharp wave, distinguishable from the background activity and lasting for 70-200 ms; spike, the same as sharp wave but with a duration of 20 to 70 ms; sharp-and-slow-wave complex, patterns consisting of a sharp followed by a slow wave; spike-and-slow-wave complex, patterns consisting of a spike followed by a slow wave; and multiple spike-and-slow-wave complex, the same as spike-and-slow-wave complex but with 2 or more spikes associated with one or more slow waves.[25] Also depending on having unilateral or bilateral IED sources the number of EEG channels with visible IEDs can be different, meaning that the IEDs have various spatial distributions. Furthermore, some IEDs are similar to artifacts (i.e. extracerebral potentials from muscle, eyes, heart, electrodes, etc.) and waves which are part of the normal background activity.[26] These properties (having different morphologies and spatial distribution as well as the IEDs similarity to artifacts and normal waves) make a great deal of uncertainty in labeling the IEDs and making the IED detection difficult. Thirty-five neurologists visually scored the IEDs from scalp-EEG.[27] The median number of IEDs labeled by these neurologists was 54 (ranging from 6 to 212 with the standard deviation of 52.3). In another study,[28] nineteen neurologists were participated in the annotation of IEDs in phase 1. The mean number of IEDs labeled by the neurologists was 58.7 (ranging from 16 to 195). A master list of 235 segments was created by including only the events which were marked as IED by at least two neurologists. In the second phase, 18 out of 19 neurologists were participated in categorizing the events in the master list. Interestingly, neurologists were inconsistent in their IED scoring between the two phases. This uncertainty can be mathematically expressed by probability of the waveform being an IED. To the best of our knowledge, there exists no study in incorporating such uncertainty in automatically detecting the IEDs. Therefore, we aim to include the IED probabilities in the design of a high dimensional tensor decomposition approach.

In this paper, IEDs are detected in two dif-

ferent approaches, subject-dependent and subject-independent classification approaches. In the first approach, we train a classifier for each subject individually. On the other hand, in the subject-independent classification approach, we train a classifier for all the subjects.

IEDs may share some features within and between the segments, whereas non-IEDs are random and there is no shared feature within or between them. Therefore, we are interested in the IED feature space. Here, we introduce two models. In the first model, we construct a three-way tensor of time, channel, and IED segment in the subject-dependent classification approach and a four-way tensor of time, channel, IED segment, and subject in the subject-independent one. Then, the tensor is decomposed into temporal, spatial, and segmental modes using the CANDECOMP/PARAFAC optimization (CP-OPT) algorithm proposed by Acar *et al.*[29] Finally, both IED and non-IED segments are projected onto the spatial factors to derive the discriminative features. This is called spatial component analysis (SCA)-based method for IED detection. In the second model, apart from the data tensor, a probability tensor is defined according to the probability of the waveform being an IED. Then, a weighted CP-WOPT (CP-WOPT)[30] is employed to obtain the tensor factors. Finally, we projected both IED and non-IED segments onto the spatial factors to extract the most significant features. This is called spatial component analysis by considering the IED probabilities (SCA-IEDP)-based method for IED detection.

The paper is organized as follows. The data recording and preprocessing, a brief review of CP-OPT and CP-WOPT algorithms, our proposed SCA and SCA-IEDP models for IED detection, feature extraction and selection, and the compared methods are presented in Section 2. Section 3 shows the experimental results. In Section 4, we discuss deeply the pros and cons of the proposed models and the compared methods. Section 5 concludes our work.

2. Methods and Experiments

2.1. *Patient Population*

The scalp and intracranial EEG signals of 18 epileptic subjects (11 males, 7 females, average age 25.2 years, and age range 13–37 years) were simultaneously recorded at King's College Hospital London. The patients suffered from temporal lobe epilepsy.

2.2. *Recording Session*

Eighteen (18) standard silver chloride electrodes were used for recoding scalp-EEG, placed on the scalp according to the 'Maudsley' electrode placement system – which is essentially similar to 10–20 system but mid-temporal, posterior-temporal and occipital electrodes in the Maudsley system are approximately 20 mm lower than in the 10–20 system in order to improve recording from the temporal lobes.[5] iEEG were recorded by using 12 intracranial multicontact FO electrodes consisting of a couple of 6 electrode bundles. The data were recorded at the sampling rate of 200 Hz and filtered by a bandpass filter with cutoff frequency of 0.3-70 Hz. Both the scalp-EEG and iEEG were recorded with respect to Pz as a common reference.

Table 1. The total number of IED and non-IED segments for each subject. The same number of IED and non-IED segments were chosen for each subject.

Subject	No. of segments	Subject	No. of segments
S1	38	S10	622
S2	524	S11	692
S3	302	S12	344
S4	108	S13	26
S5	158	S14	20
S6	648	S15	692
S7	250	S16	22
S8	552	S17	178
S9	38	S18	338

2.3. *Preprocessing*

For each patient, we analyzed 20 minutes of scalp recordings to include the IEDs only and avoid postictal slowing or flattening. A bandpass filter over 4-48 Hz was applied to the scalp-EEG signals in order to increase the signal-to-noise ratio. We selected the highpass frequency to be 4 Hz to remove eye blink artifacts and the lowpass frequency to be 48 Hz in order to preserve the IEDs' morphology as IEDs are likely to have high frequency components.

For analysis and classification, the EEG signals were sliced. The length of IED segments was selected to be 480 ms (96 time sample) – 160 ms before and 320 ms after the positions of peaks in iEEG marked as IED. Non-IED segments with 480 ms length were selected from time segments where there were no

scored IEDs. We chose the same number of IED and non-IED segments for each subject. Both IED and non-IED segments were linearly detrended to remove the undesired drifts. The total number of IED and non-IED segments is illustrated in Table 1. Subjects 13, 14, and 16 were excluded from analysis because of having less number of segments.

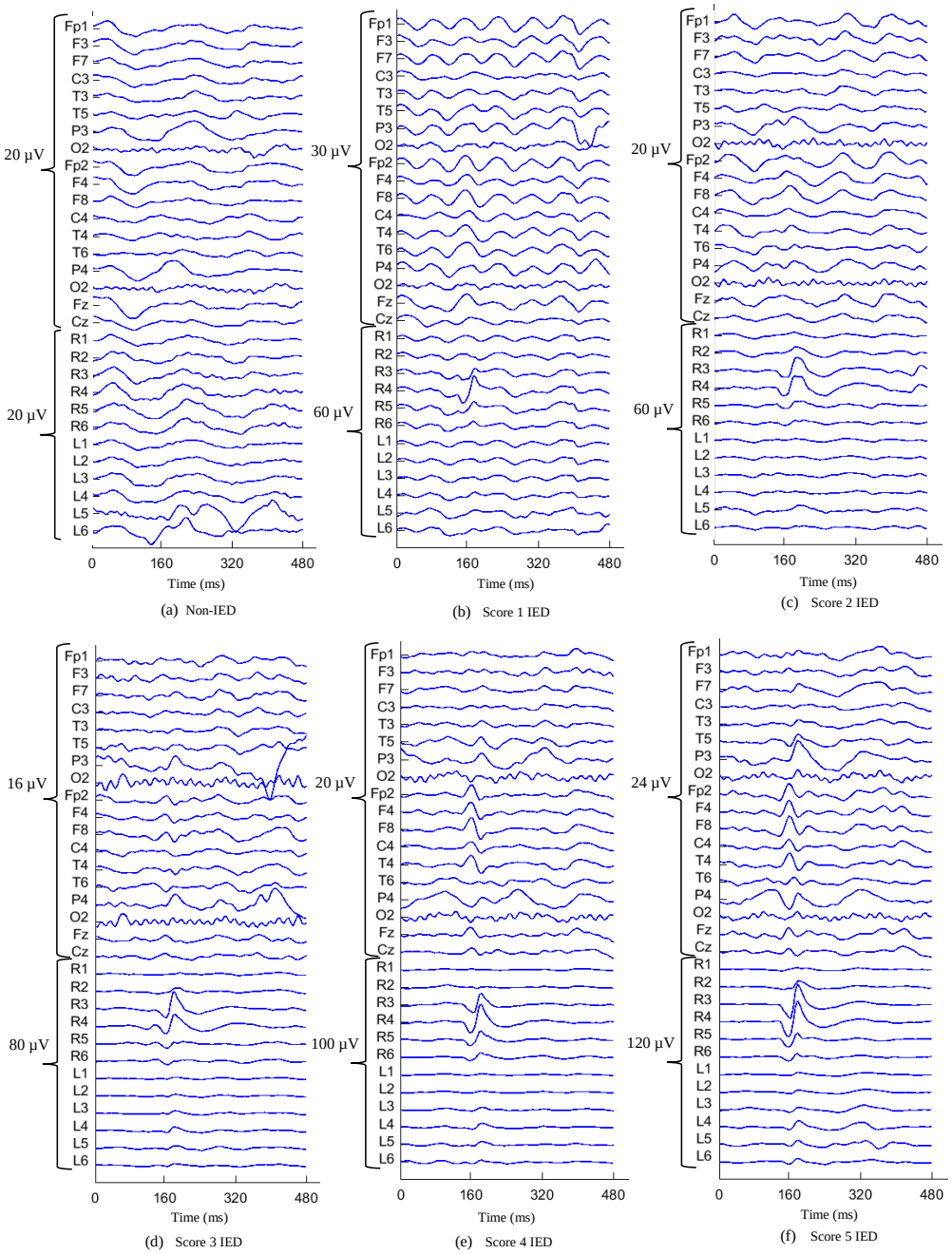

Figure 1. Samples of non-IED and IED waveforms with scores 1 to 5. (a) The IED with score 1, and (b)-(f) Respectively the IED with score 1 to 5 (score 5 refers to an IED with the highest probability (or the lowest uncertainty)). An expert epileptologist used the iEEG as ground truth in scoring IEDs. The IEDs start at 160ms.

2.4. *IED Scoring*

The iEEG was used as the ground truth for scoring the IEDs by an expert epileptologist who scored the IEDs based on the morphology and spatial distribution of the observed waveforms and gave a score between 1 (for low certainty) to 5 (for high certainty) for each IED. Score 1 refers to the lowest probability of the waveform being an IED, meaning that the epileptologist is not certain whether the activity is an IED or not. Score 5 denotes the highest probability of being an IED, meaning that they are certainly related to the IED activities. Fig. 1 shows samples of non-IED and IED waveforms with scores 1 to 5. No spike or sharp wave can be seen in the non-IED segment. In the IED segment scored 1, there is a sharp wave in the FO channel. A couple of FO channels contain sharp waves in the IED segment scored 2. However, no spike or sharp wave is observable over the scalp for IEDs scored 1 or 2. There are spikes in a couple of FO channels in the IED segment scored 3 and, by referencing to FO channels, some broad waves can be seen on few scalp channels. These segments (with IEDs scored 1, 2, or 3) have been marked as scalp-invisible IEDs. On the other hand, in the IEDs scored 4 or 5, there are spike waves in many FO and scalp channels with higher amplitudes. These have been marked as scalp-visible IEDs.

2.5. *IED Detection Based on SCA*

In SCA, CP-OPT[29] is employed to decompose the data. We first give a brief description of CP-OPT algorithm. Then, we adopt the algorithm to exploit the spatial factors among the IED segments in two different approaches so as to solve our IED detection problem.

The notation used in this paper has been adopted from Ref.[31] lowercase letters, e.g., a, denotes scalars. Boldface lowercase letters, e.g., $\mathbf{a}$, represent vectors. Boldface capital letters, e.g., $\mathbf{A}$, denote matrices. Boldface Euler script letters, e.g., $\boldsymbol{\mathcal{X}}$, denote higher-order tensors. $\mathbf{a}_j$ denote the j-th column of matrix $\mathbf{A}$. The symbols '$\circ$' and '$*$' represent respectively the vector outer product and the elementwise product, and $\odot$ denotes the Khatri-Rao product.

2.5.1. *CP-OPT*

Suppose we are given an N-way tensor $\boldsymbol{\mathcal{X}} \in \mathbb{R}^{I_1 \times I_2 \times \cdots \times I_N}$. We aim to factorize the tensor into sum of rank-one tensors as follows:

$$\boldsymbol{\mathcal{X}} \approx \sum_{r=1}^{R} \mathbf{a}_r^{(1)} \circ \cdots \circ \mathbf{a}_r^{(N)}, \tag{1}$$

where $\mathbf{a}_r^{(n)} \in \mathbb{R}^{I_n}$ for $n = 1, \ldots, N$ and $r = 1, \ldots, R$ (R is the number of components). The factor matrices are constructed from the combination of vectors from the rank-one components, i.e., $\mathbf{A}^{(n)} = \left[\mathbf{a}_1^{(n)} \cdots \mathbf{a}_R^{(n)}\right]$. Following the "Kruskal operator",[32] we can rewrite (1) as

$$\boldsymbol{\mathcal{X}} \approx [\![\mathbf{A}^{(1)}, \ldots, \mathbf{A}^{(N)}]\!] \equiv \sum_{r=1}^{R} \mathbf{a}_r^{(1)} \circ \cdots \circ \mathbf{a}_r^{(N)}. \tag{2}$$

The problem of computing CP (2) can be formulate as a least-square optimization problem:

$$\min_{\mathbf{A}^{(1)}, \ldots, \mathbf{A}^{(N)}} f \equiv \frac{1}{2} \left\| \boldsymbol{\mathcal{X}} - [\![\mathbf{A}^{(1)}, \ldots, \mathbf{A}^{(N)}]\!] \right\|^2. \tag{3}$$

Unlike the alternating least-squares approach[33] solving the factor matrices one by one, the CP-OPT algorithm developed by Acar *et al.*[29] solves all the factor matrices simultaneously using a gradient-based optimization approach. It is straightforward to derive the gradient of objective function f by calculating the partial derivatives with respect to each $\mathbf{A}^{(n)}$, i.e.,

$$\frac{\partial f}{\partial \mathbf{A}^{(n)}} = -\mathbf{X}_{(n)} \mathbf{A}^{(-n)} + \mathbf{A}^{(n)} \boldsymbol{\Gamma}^{(n)}, \tag{4}$$

for $n = 1, \ldots, N$, in which $\mathbf{X}_{(n)}$ is the mode-n matricization of the tensor $\boldsymbol{\mathcal{X}}$; $\mathbf{A}^{(-n)}$ is defined as

$$\mathbf{A}^{(-n)} \equiv \mathbf{A}^{(N)} \odot \cdots \mathbf{A}^{(n+1)} \odot \mathbf{A}^{(n-1)} \odot \cdots \odot \mathbf{A}^{(1)}; \tag{5}$$

and $\boldsymbol{\Gamma}^{(n)}$ is defined as

$$\boldsymbol{\Gamma}^{(n)} = \boldsymbol{\Upsilon}^{(1)} * \cdots * \boldsymbol{\Upsilon}^{(n-1)} * \boldsymbol{\Upsilon}^{(n+1)} * \cdots * \boldsymbol{\Upsilon}^{(N)}, \tag{6}$$

where $\boldsymbol{\Upsilon}^{(n)} = \mathbf{A}^{(n)T} \mathbf{A}^{(n)}$.

To see the proof of (4) the reader is referred to Ref.[29] Once the gradients are known, any gradient-based method can be used to solve the optimization problem. In this paper, the nonlinear conjugate gradient method[34] is used.

2.5.2. *Detecting IEDs Using SCA in the Subject-dependent Approach*

In the subject-dependent classification approach, a classifier is trained and validated using the data from the same subject.

As IEDs are abnormal activity and independent from the other activities, their feature space does not involve other brain activities. Therefore, we aim

to estimate a feature space spanning over only the IED segments. Suppose we are given N IED segments (N_1 for training and N_2 as test data) and H non-IED segments. We construct a three-way tensor, $\boldsymbol{\mathcal{X}} \in \mathbb{R}^{L\times M\times N_1}$ (whose dimensions L, M, and N_1 correspond respectively to time, channel, and IED segment).

CP-OPT is applied to the tensor $\boldsymbol{\mathcal{X}}$, as:

$$\min_{\mathbf{A},\mathbf{B},\mathbf{C}} \quad f \equiv \frac{1}{2}\left\|\boldsymbol{\mathcal{X}} - [\![\mathbf{A},\mathbf{B},\mathbf{C}]\!]\right\|^2, \tag{7}$$

to obtain the factor matrices, where $\mathbf{A} \in \mathbb{R}^{L\times R}$ and $\mathbf{B} \in \mathbb{R}^{M\times R}$ represent respectively the temporal and spatial factors, and $\mathbf{C} \in \mathbb{R}^{N_1\times R}$ corresponds to the segmental factor. Then, both the IED and non-IED segments are projected onto the spatial factor $\mathbf{B}$ as follows:

$$\mathbf{P}_k = \mathbf{X}_k\mathbf{B} \tag{8}$$

where $\mathbf{X}_k \in \mathbb{R}^{L\times M}(k = 1,\ldots,N,1,\ldots,H)$ is an IED or non-IED segment from the training or test data and $\mathbf{P}_k \in \mathbb{R}^{L\times R}(k = 1,\ldots,N,1,\ldots,H)$ is the projected IED or non-IED segment.

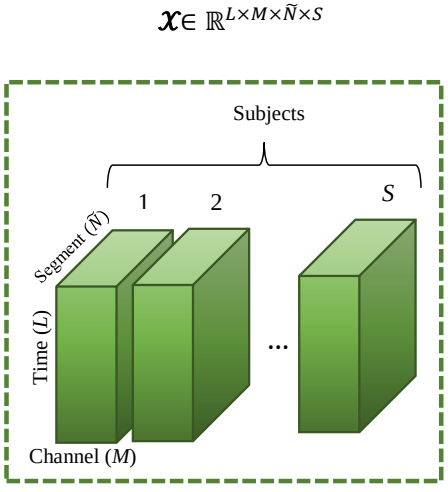

Figure 2. The four-way tensor constructed by concatenating three-way tensors of S subjects.

2.5.3. *Detecting IEDs Using SCA in the Subject-independent Approach*

In the subject-independent classification approach, a number of subjects are used for training a classifier. Then, the classifier is validated using new subjects. The three-way tensors of subjects are concatenated into a single four-way tensor $\boldsymbol{\mathcal{X}} \in \mathbb{R}^{L\times M\times \widetilde{N}\times S}$, where $\widetilde{N}$ denotes the number of IED segments supposed to be selected equally for all the training subjects and S is the number of subjects in the training dataset. Fig. 2 shows the schematic of the four-way tensor.

CP-OPT is employed to decompose tensor $\boldsymbol{\mathcal{X}}$ to its factor matrices:

$$\min_{\mathbf{A},\mathbf{B},\mathbf{C},\mathbf{D}} \quad f \equiv \frac{1}{2}\left\|\boldsymbol{\mathcal{X}} - [\![\mathbf{A},\mathbf{B},\mathbf{C},\mathbf{D}]\!]\right\|^2, \tag{9}$$

where $\mathbf{A}$ and $\mathbf{B}$ represent respectively the temporal and spatial factors, and $\mathbf{C} \in \mathbb{R}^{\widetilde{N}\times R}$ and $\mathbf{D} \in \mathbb{R}^{S\times R}$ correspond respectively to the segmental and individual (subject) factors.

Finally, both IED and non-IED segments of the training and test subjects are projected onto the spatial factor as follow:

$$\mathbf{P}_{\widetilde{k}} = \mathbf{X}_{\widetilde{k}}\mathbf{B} \tag{10}$$

where $\mathbf{X}_{\widetilde{k}} \in \mathbb{R}^{L\times M}(\widetilde{k} = 1,\ldots,\widetilde{K})$ is an IED or non-IED segment from the training or test subjects and $\mathbf{P}_{\widetilde{k}} \in \mathbb{R}^{L\times R}(\widetilde{k} = 1,\ldots,\widetilde{K})$ is the projected IED or non-IED segment.

2.6. *IED Detection Based on SCA-IEDP*

In the proposed SCA-IEDP method, the CP-WOPT[30] is utilized to extract spatial factors among the IED segments with different probabilities.

2.6.1. *CP-WOPT*

Let $\boldsymbol{\mathcal{X}}$ be an N-way tensor with the dimension of $I_1 \times I_2 \times \cdots \times I_N$. In CP-WOPT, we define a weight tensor $\boldsymbol{\mathcal{W}}$ of the same size as $\boldsymbol{\mathcal{X}}$ such that $\{0 \le w_{i_1 i_2 \cdots i_N} \le 1\}$ for all $i_n \in 1,\ldots,I_n$ and $n \in 1,\cdots,N$.

The optimization for the general N-way CP-OPT factorization in (3) changes to

$$\min_{\mathbf{A}^{(1)},\ldots,\mathbf{A}^{(N)}} f_w \equiv \tfrac{1}{2}\left\|\boldsymbol{\mathcal{W}} * (\boldsymbol{\mathcal{X}} - [\![\mathbf{A}^{(1)},\ldots,\mathbf{A}^{(N)}]\!])\right\|^2. \tag{11}$$

The above optimization problem may be reformulated to

$$\min_{\mathbf{A}^{(1)},\ldots,\mathbf{A}^{(N)}} f_w \equiv \frac{1}{2}\left\|\boldsymbol{\mathcal{Y}} - \boldsymbol{\mathcal{Z}}\right\|^2, \tag{12}$$

where $\boldsymbol{\mathcal{Y}} = \boldsymbol{\mathcal{W}} * \boldsymbol{\mathcal{X}}$ and $\boldsymbol{\mathcal{Z}} = \boldsymbol{\mathcal{W}} * [\![\mathbf{A}^{(1)},\ldots,\mathbf{A}^{(N)}]\!]$.

We aim to find the factor matrices $\mathbf{A}^{(n)} \in \mathbb{R}^{I_n\times R}$, for $n = 1,\ldots,N$, which minimize the weighted objective function in (12). We derive the gradient in (12) by calculating the partial derivatives

of f_w with respect to each factor matrix $\mathbf{A}^{(n)}$ as follows:

$$\frac{\partial f_w}{\partial \mathbf{A}^{(n)}} = \left(\mathbf{Z}_{(n)} - \mathbf{Y}_{(n)}\right) \mathbf{A}^{(-n)}, \tag{13}$$

for $n = 1, \ldots, N$, where $\mathbf{A}^{(-n)}$ is defined in (5).

The detailed proof of (13) is expressed in Ref.[30] After calculating the partial derivatives using (13), any gradient-based optimization method can be utilized to solve the optimization problem.

2.6.2. *Detecting IEDs Using SCA-IEDP in the Subject-dependent Approach*

Like in Section 2.5.2, we train and validate a classifier within the subjects. Apart from the data tensor, in SCA-IEDP, we define a probability tensor $\boldsymbol{\mathcal{W}}$ of the same size as $\boldsymbol{\mathcal{X}}$ based on the IED probabilities as follows:

$$\begin{cases} \mathbf{W}_{::n_1} = c_1 & \text{for case 1} \\ \mathbf{W}_{::n_1} = c_2 & \text{for case 2} \\ \vdots & \\ \mathbf{W}_{::n_1} = c_{J-1} & \text{for case } J-1 \\ \mathbf{W}_{::n_1} = c_J & \text{for case } J, \end{cases} \tag{14}$$

for all $n_1 = 1, \ldots, N_1$, where $\{0 \leq c_j \leq 1\}$ for $j \in \{1, \ldots, J\}$ and $\mathbf{W}_{::n_1}$ are the frontal slices of $\boldsymbol{\mathcal{W}}$. The cases are defined based on spatial distribution and morphology of IEDs by expert epileptologists.

The CP-WOPT algorithm is applied to the data tensor $\boldsymbol{\mathcal{X}}$ and probability tensor $\boldsymbol{\mathcal{W}}$, as:

$$\min_{\mathbf{A},\mathbf{B},\mathbf{C}} f_w \equiv \frac{1}{2} \left\| \boldsymbol{\mathcal{W}} * \left(\boldsymbol{\mathcal{X}} - [\![\mathbf{A}, \mathbf{B}, \mathbf{C}]\!]\right) \right\|^2, \tag{15}$$

to obtain the factor matrices, where $\mathbf{A}, \mathbf{B}$ and $\mathbf{C}$ correspond respectively to the temporal, spatial, and segmental factors. Then, both the IED and non-IED segments are projected onto the spatial factor $\mathbf{B}$ using (8). Finally, the projected IEDs and non-IEDs, $\mathbf{P}_k$, are used for classification. The flow diagram of the proposed models in the subject-dependent approach is illustrated in Fig. 3.

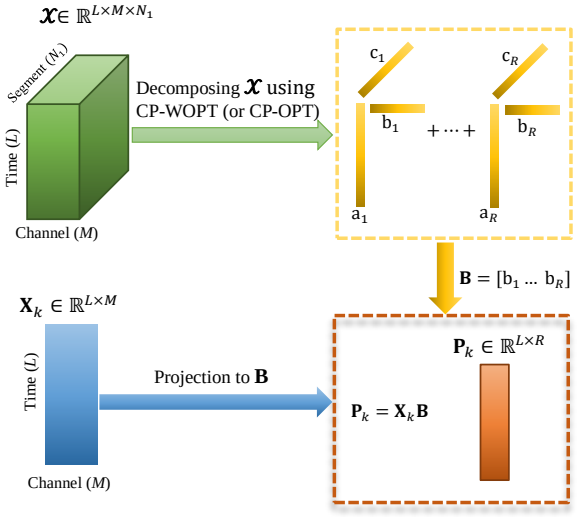

Figure 3. The IED detection system proposed for the subject-dependent classification approach. $\boldsymbol{\mathcal{X}}$ includes the IED segments only, N_1. CP-OPT (or CP-WOPT) is applied to $\boldsymbol{\mathcal{X}}$ to decompose it to temporal, spatial, and segmental factors. $\mathbf{X}_k (k = 1, \ldots, N, 1, \ldots, H)$ is an IED or non-IED segment from the training or test data, which is projected onto the spatial components $\mathbf{B}$. $\mathbf{P}_k$ represents the same segment after projection.

2.6.3. *Detecting IEDs Using SCA-IEDP in the Subject-independent Approach*

Apart from the four-way data tensor $\boldsymbol{\mathcal{X}}$ described in Section 2.5.3 and shown in Fig. 2, a four-way probability tensor $\boldsymbol{\mathcal{W}}$ is also defined. The three-way probability tensors of the training subjects described in (14) are concatenated into a single four-way tensor, called four-way probability tensor $\boldsymbol{\mathcal{W}}$.

The CP-WOPT algorithm is employed to decompose the data tensor $\boldsymbol{\mathcal{X}}$ and probability tensor $\boldsymbol{\mathcal{W}}$, as illustrated below, into the factor matrices:

$$\min_{\mathbf{A},\mathbf{B},\mathbf{C},\mathbf{D}} f_w \equiv \frac{1}{2} \left\| \boldsymbol{\mathcal{W}} * \left(\boldsymbol{\mathcal{X}} - [\![\mathbf{A}, \mathbf{B}, \mathbf{C}, \mathbf{D}]\!]\right) \right\|^2. \tag{16}$$

Finally, both the IED and non-IED segments are projected onto the spatial factor $\mathbf{B}$ using (10), and the projected IEDs and non-IEDs, $\mathbf{P}_{\widetilde{k}}$, are used for classification.

In the classification stage, all IEDs with different scores fall within the same IED class. However, we define a probability tensor $\boldsymbol{\mathcal{W}}$ based on these scores, which gives an opportunity to incorporate the probability of a waveform being an IED in our IED detection system.

2.7. *Feature Extraction*

The proposed models are applied to detect IEDs from the scalp-EEG signals. The concurrent intracranial data is used as the ground truth by an expert epileptologist for scoring IEDs. The temporal and spatial resolutions of scalp-EEG and iEEG are generally different. However, the correlation between scalp-EEG and iEEG does not affect our model since they are not combined in the analysis (iEEG is used for manually scoring scalp-visible and scalp-invisible IEDs and scalp-EEG is employed to detect IEDs from over the scalp).

2.7.1. *Feature Extraction in the Subject-dependent Approach*

We construct a three-way tensor $\boldsymbol{\mathcal{X}} \in \mathbb{R}^{96\times 18\times N_1}$, where 96 and 18 are respectively time samples and the number of recorded channels and $N1$ denotes the number of IED segments in the training fold. Apart from the IEDs tensor, we build a tensor $\boldsymbol{\mathcal{W}}$ with the same dimension as tensor $\boldsymbol{\mathcal{X}}$ in the SCA-IEDP model to which different certainty levels are allocated as follows:

$$\begin{cases} \mathbf{W}_{::n_1} = 0.2 & \text{If the IED is given score 1} \\ \mathbf{W}_{::n_1} = 0.6 & \text{If the IED is given score 2} \\ \mathbf{W}_{::n_1} = 0.8 & \text{If the IED is given score 3} \\ \mathbf{W}_{::n_1} = 0.9 & \text{If the IED is given score 4} \\ \mathbf{W}_{::n_1} = 1 & \text{If the IED is given score 5,} \end{cases}$$

for $n_1 = 1, \ldots, N_1$, where the groups are defined according to Section 2.4. $\mathbf{W}_{::n_1} = 0.2$ means that the waveform is related to an IED activity for 20% and it is related to a non-IED activity for 80%. $\mathbf{W}_{::n_1} = 0.6$ means that the waveform is an IED activity for 60% and it is a non-IED activity for 40% and so on.

The tensor is decomposed separately using CP-OPT and CP-WOPT to extract the factor matrices:

$$\boldsymbol{\mathcal{X}} \approx \sum_{r=1}^{R} \mathbf{a}_r \circ \mathbf{b}_r \circ \mathbf{c}_r \equiv [\![\mathbf{A}, \mathbf{B}, \mathbf{C}]\!],$$

where $\mathbf{A} \in \mathbb{R}^{96\times R}$ and $\mathbf{B} \in \mathbb{R}^{18\times R}$ denote respectively the temporal and spatial factors, and $\mathbf{C} \in \mathbb{R}^{N_1\times R}$ is the segmental factor. Then, both the IED and non-IED segments are projected onto the spatial factor $\mathbf{B}$ using (8), where $\mathbf{X}_k \in \mathbb{R}^{96\times 18}$ is an IED or non-IED segment from the training or test data and $\mathbf{P}_k \in \mathbb{R}^{96\times R}$ is the projected IED or non-IED segment.

Time-frequency representations have been broadly and successfully used in IED detection[19] and epilepsy diagnosis.[35,36] The spectrogram method is applied to the projected IEDs and non-IEDs, $\mathbf{P}_k$, to extract the time-frequency features. The magnitudes of short-time Fourier transform obtained using the spectrogram are measured and used as features. For the spectrogram, we define a Hanning window size of 80 ms (16 samples) and an overlap of 50% (8 samples). Overall, 11 windows slide over the segments. The number of discrete Fourier transform points has been set to 16 (the same as the number of time samples in a window) resulting in 9 frequency features. Totally, we obtained $R \times 11 \times 9$ features, where R is the number of spatial components extracted using the tensor, 11 is the number of time slabs, and 9 is the number of frequency slabs for each IED or non-IED segment.

2.7.2. *Feature Extraction in the Subject-independent Approach*

After concatenating the three-way tensors into a four-way tensor $\boldsymbol{\mathcal{X}} \in \mathbb{R}^{96\times 18\times 30\times S}$ and defining $\boldsymbol{\mathcal{W}}$ for CP-WOPT, we decompose $\boldsymbol{\mathcal{X}}$ using CP-OPT and CP-WOPT, separately, into temporal $\mathbf{A} \in \mathbb{R}^{96\times R}$, spatial $\mathbf{B} \in \mathbb{R}^{18\times R}$, segmental $\mathbf{C} \in \mathbb{R}^{30\times R}$, and individual (subject) $\mathbf{D} \in \mathbb{R}^{S\times R}$ factors. We randomly selected 30 IED segments from each training subject. (Therefore, those subjects having at least 30 IED segments and providing a reasonable performance in the subject-dependent approach were chosen as the training subjects). Then, both the IED and non-IED segments of the training and test subjects are projected onto the spatial factor. Finally, time-frequency features of the projected IEDs and non-IEDs are calculated using the spectrogram.

2.8. *Number of Components*

Finding the number of components plays an important role in tensor decomposition, and it is also an NP-hard problem. However, in order to determine the number of suitable components R, we apply nested cross validation. The training data are split into 5-fold. Each time 4 folds are used for training the model and the fifth fold for validation. The nested cross validation was performed for $R = \{1, 2, 3, 4\}$. In each case $R = \{1, 2, 3, 4\}$, the accuracy was averaged across 5 folds. Finally, the number of compo-

nents is determined based on the highest accuracy. In our work, the minimum number of components was one ($R = 1$) and the maximum number was four ($R = 4$), depending on how many components gave the best performance. It is worth noting that the nested cross validation is performed over the training dataset only. The test dataset is not contributed in determining the number of components.

2.9. *Compared Methods*

We compare the performance of our proposed approaches with two other state-of-the-art methods in IED detection namely, time-frequency (TF) features[19] and simultaneous multilinear low-rank approximation of tensors (SMLRAT).[24]

2.9.1. *Time-frequency Features Model*

We already discovered that the TF features show an improvement over continuous wavelet transform (CWT) and chirplet transform for this particular dataset.[19] Therefore, we compare our proposed models with a model based on TF features, which is obtained by employing the spectrogram method – calculated following Section 2.7. Each IED or non-IED segment was made of 1782 features (18 scalp channels $\times$11 temporal $\times$9 frequency).

2.9.2. *Simultaneous Multilinear Low-rank Approximation of Tensors*

We compare the proposed approaches with SMLRAT proposed recently by Thanh *et al.* for EEG epileptic spike detection.[24] The model is based on NTD.

In the SMLRAT, the authors applied CWT to the epileptic and non-epileptic spikes and constructed a three-way tensor for each segment, $\boldsymbol{\mathcal{X}}_i \in \mathbb{R}^{W\times L\times M}$, where $W, L,$ and M denote respectively wavelet-scale, time, and channel. They concatenated only three-way tensors, $\{\boldsymbol{\mathcal{X}}_i^{ep}\}_{i=1}^{N_1}$, where N_1 represents the number of epileptic spike segments, in a single four-way tensor $\widetilde{\boldsymbol{\mathcal{X}}}^{ep} \in \mathbb{R}^{W\times L\times M\times N_1}$. Then, NTD was employed to decompose the tensor $\widetilde{\boldsymbol{\mathcal{X}}}^{ep}$ and obtain the factor matrices:

$$\widetilde{\boldsymbol{\mathcal{X}}}^{ep} = \widetilde{\boldsymbol{\mathcal{X}}}_1^{ep} \boxplus \widetilde{\boldsymbol{\mathcal{X}}}_2^{ep} \cdots \boxplus \widetilde{\boldsymbol{\mathcal{X}}}_{N_1}^{ep} = \boldsymbol{\mathcal{G}} \times_1 \mathbf{U} \times_2 \mathbf{A} \times_3 \mathbf{B} \times_4 \mathbf{C}, \quad (17)$$

where $\boldsymbol{\mathcal{G}} \in \mathbb{R}^{r_1\times r_2\times r_3\times N_1}$ is the core tensor, and $\mathbf{U} \in \mathbb{R}^{W\times r_1}, \mathbf{A} \in \mathbb{R}^{L\times r_2}, \mathbf{B} \in \mathbb{R}^{M\times r_3}$, and $\mathbf{C} \in \mathbb{R}^{N_1\times N_1}$ denote respectively the wavelet-scale, time, channel, and epileptic spikes. Finally, in order to obtain the feature space of each segment, the epileptic and non-epileptic spikes were projected onto the factor matrices as follows:

$$\boldsymbol{\mathcal{F}}_i = \boldsymbol{\mathcal{X}}_i \times_1 \mathbf{U}^\dagger \times_2 \mathbf{A}^\dagger \times_3 \mathbf{B}^\dagger, \quad (18)$$

where $(.)^\dagger$ represents matrix Moore-Penrose pseudo-inverse.

Here, we decompose the IED and non-IED segments through CWT and construct a three-way tensor for each segment – $\boldsymbol{\mathcal{X}}_i \in \mathbb{R}^{38\times 96\times 18}$. We concatenate three-way IED tensors into a single four-way tensor, then perform NTD to obtain the factors; $\mathbf{U} \in \mathbb{R}^{38\times 10}, \mathbf{A} \in \mathbb{R}^{96\times 15}$, and $\mathbf{B} \in \mathbb{R}^{18\times 18}$; and consequently the features $\boldsymbol{\mathcal{F}}_i \in \mathbb{R}^{10\times 15\times 18}$.

2.10. *Feature Selection*

In our proposed models, we use all the features for classification since we have at most 396 features subject to $R = 4$. Nevertheless, there are a large number of features in the compared methods, 1782 features in TF and 2700 features in SMLRAT. For having a fair comparison, we select the significant features based on the Fisher score algorithm, which was used as the feature selection method in the referenced SMLRAT paper.[24] Fisher score is defined as follows:

$$\varphi_q = \frac{\sum_{c=1}^{c=C} n_c(\mu_{qc} - \mu_q)^2}{\sum_{c=1}^{c=C} n_c \rho_{qc}^2} \quad (19)$$

where μ_{qc} and ρ_{qc} are respectively the mean and variance of the q-th feature in the c-th class, n_c is the number of instances in the c-th class, and μ_q is the mean of the q-th feature.

2.11. *Classification*

In order to classify the IED and non-IED segments, we employed four different classifiers, namely diagonal linear discriminant analysis (DLDA), naïve Bayes (NB), support vector machines (SVM), and decision tree ensembles (DTE). DLDA is superior to LDA in high-dimensional problems. The covariance matrix needs to be computed in LDA. Calculating all the covariance matrix terms in a high-dimensional case may fail due to small data size. A strong independence assumption may be applied to the features resulting a diagonal covariance matrix in LDA. This modification of LDA is called DLDA. We have feature independence assumption in NB as well. SVM is

a popular classifier often used for seizure EEG classification.[37,38] In these cases, linear SVM is more applicable than nonlinear (kernel-based) SVM due to separability of the data and avoiding overfitting. The DTE classifier has been the last one that we utilized. The feasibility of ensemble classification methods in EEG classification has been proven.[39] We have used bagging technique to perform ensemble decision trees.[40] In the bagging method, the idea is to create several subsets of data from the training samples which is randomly selected with replacement. Then, each subset is employed to train its decision tree. Hence, we end up with an ensemble of different models, where the average of all the predictions from different trees are used, which is more robust than each single decision tree.

2.12. *Evaluation and Cross Validation*

We employed a k-fold (k=5) cross validation to validate the methods in the subject-dependent classification approach. Four folds were used for training the models and the fifth fold as the test data. Increasing the number of folds did not change the outcome. It is worth emphasizing that the classifiers are trained and tested using only scalp-EEG. In the subject-independent approach, the leave-subject-out cross validation was employed. The data of a subject used as the test data, other subjects data were used for training the classifiers.

For evaluation the methods, accuracy (ACC), sensitivity (SEN), specificity (SPEC), and F1 score (F1-S) were obtained as follows:

$$\text{ACC} = \frac{TP + TN}{TP + FP + TN + FN} \times 100\%, \quad (20)$$

$$\text{SEN} = \frac{TP}{TP + FN} \times 100\%, \quad (21)$$

$$\text{SPEC} = \frac{TN}{TN + FP} \times 100\%, \quad (22)$$

$$\text{F1-S} = \frac{2TP}{2TP + FP + FN}, \quad (23)$$

where TP is the number of IED samples classified correctly in the IED class, TN represents the number of non-IED samples recognized accurately as non-IED samples, FP indicates the number of non-IED samples detected incorrectly as IED samples, and FN indicates the number of IED samples categorized wrongly in the non-IED class. Accuracy shows the percentage of detection of IED and non-IED samples, and sensitivity and specificity illustrate the ability of the classifiers in correctly detecting the IED and non-IED samples, respectively.

3. Results

Here, we firstly analyze the temporal and spatial components of CP-OPT and CP-WOPT decomposition. We employed four types of classifiers to detect IEDs. Next, we present the obtained results of our proposed SCA and SCA-IEDP models and of the compared methods in the subject-dependent classification approach. Finally, we report the obtained results of SCA, SCA-IEDP, and SMLRAT in the subject-independent classification approach.

3.1. *Analysis of Temporal and Spatial Factors*

The first temporal factors of CP-OPT and CP-WOPT are illustrated in Fig. 4(a). The temporal factor of CP-WOPT not only has higher amplitude than that of CP-OPT but also is sharper. It is due to the fact that, in CP-WOPT, those IEDs having spike or spike-and-slow-wave complex morphology are given greater weight than those having sharp wave morphology. Whereas, in CP-OPT, all IEDs with different morphologies are given the same weight.

In addition, the spatial distributions of the first factors of CP-OPT and CP-WOPT were computed and are respectively shown in Figs. 4(b) and 4(c). The spatial distribution of CPWOPT is more focal and right laterally distributed than that of CP-OPT as expected.

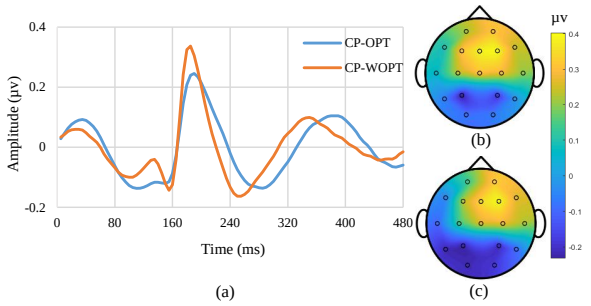

Figure 4. The first temporal components and spatial distributions obtained using CP-OPT and CP-WOPT: (a) The temporal components, (b) and (c) the spatial distributions obtained respectively by CP-OPT and CP-WOPT.

Table 2. The performance of classifiers with results averaged over all subjects and folds. The classifiers were trained and tested in the subject-dependent classification approach. ACC, SEN, and SPEC are presented in percent %.

Classifiers	Models	ACC	SEN	SPEC	F1-S
NB	TF	70.5	68	73	0.68
	SMLRAT	71.3	61.7	80.1	0.65
	SCA	78.1	70.3	86	0.75
	SCA-IEDP	**79.2**	**71.3**	**87**	**0.76**
DLDA	TF	70.7	61	80.3	0.66
	SMLRAT	64.9	46.4	83.4	0.54
	SCA	75.3	61.7	**88.9**	0.7
	SCA-IEDP	**76**	**63.1**	**88.8**	**0.71**
SVM	TF	66.9	65.2	68.2	0.66
	SMLRAT	72.9	63.8	82	0.69
	SCA	78.9	70.8	**87**	**0.76**
	SCA-IEDP	**79.2**	**71.4**	**87**	**0.76**
DTE	TF	73	66.2	79.8	0.69
	SMLRAT	72.7	70.9	74.5	0.70
	SCA	78.3	73.9	**82.8**	0.76
	SCA-IEDP	**79.9**	**77.6**	82.1	**0.79**

3.2. *IED detection in the subject-dependent classification approach*

Table 2 illustrates the classification results for the subject-dependent approach. We compare our proposed SCA and SCA-IEDP models with TF and SMLRAT methods developed quite recently. It is worth noting that the first 200 significant features of the TF and the first 100 ones of SMLRAT were classified, giving the highest accuracy in their methods.

Using NB classifier, SCA-IEDP detected IEDs and non-IEDs with 79.2% accuracy, which was approximately 1%, 8% and 9% higher than SCA, SMLRAT, and TF accuracy values, respectively. SCA-IEDP provided 73.1% SEN and 87% SPEC which was better than SCA and the compared methods as well. In DLDA, SCA-IEDP provided the best ACC of 76% and SEN of 63.1%. In contrast, its performance was comparable with SCA performance in terms of SPEC criterion.

Using SVM, the best accuracy of 79.2% and sensitivity of 71.4% were obtained using our proposed SCA-IEDP model. However, SCA and SCA-IEDP presented the same values of SPEC and F1-S. In this classifier, the TF model was the worst one in all criteria except in SEN which SMLRAT provided the worst value in. In the DTE classifier, SCA-IEDP presented the best accuracy of 79.9%, sensitivity of 77.6%, and F1-score of 0.79 though the best specificity of 82.8 was provided by SCA.

Table 2 shows that the best accuracy has been achieved by SCA-IEDP using DTE classifier. It provided 79.9% accuracy while the best accuracy values presented by SCA, SMLRAT, and TF were respectively 78.9%, 72.9%, and 73%. Overall, SPEC values were higher than SEN values in all detection methods and all classifiers, showing that the non-IED segments can be detected easier than the IED segments. SMLRAT, SCA, and SCA-IEDP provided their best SEN values using DTE classifier while TF obtained its best SEN using NB classifier. Generally, DTE presented the best trade-off between SEN and SPEC in all methods.

3.3. *IED detection in the subject-independent classification approach*

Apart from classifying IEDs and non-IEDs in the subject-dependent classification approach, the proposed SCA and SCA-IEDP models and SMLRAT are employed to detect IEDs in the subject-independent one. The obtained results are shown in Table 3. In SMLRAT,[24] the authors classified epileptic and non-epileptic spikes by concatenating the three-way tensors (time, wavelet-scale, channel) of all subjects into a single four-way tensor, and they used leave-one-subject-out cross validation. The TF model proposed in Ref.[19] detected IEDs in the subject-independent classification approach by using the ensemble of individual classifiers, rather than by combining the subjects' data. Therefore, TF is not reported here.

SCA-IEDP presented the best accuracy in all classifiers. It obtained its best accuracy, 63.4%, using both SVM and DTE classifiers. SCA-IEDP and SCA provided significantly better performance than SMLRAT. In all classifiers, the accuracy of SCA-IEDP and SCA was approximately 9-13% higher than that of SMLRAT. In NB and DLDA, SCA-IEDP provided respectively the best accuracy of 62.4% and 62.5% while the best SEN of 80% and 98.5% were obtained via the SMLRAT model. In these classifiers, most segments were recognized as IEDs through the SMLRAT model, meaning that the model was biased toward the IED class. On the other hand, SCA presented the best SPEC when NB, DLDA, and

SVM classifiers were employed, which means that the model was biased toward the non-IED class. Generally, the best trade-off between SEN and SPEC was obtained using DTE classifier in which SCA-IEDP outperformed SCA and SMLRAT in all criteria. In addition, the performance of SMLRAT was around the chance level (which is 50% for a binary classification).

Table 3. The performance of SCA, SCA-IEDP and SMLRAT models obtained using the classifiers in the subject-independent classification approach. The results have been averaged over 15 subjects. ACC, SEN, and SPEC are presented in percent %.

Classifiers	Models	ACC	SEN	SPEC	F1-S
NB	SMLRAT	49.2	**80**	17.4	**0.61**
	SCA	58.2	37.4	**79.1**	0.39
	SCA-IEDP	**62.4**	56	68.7	0.52
DLDA	SMLRAT	50	**98.5**	1.6	**0.66**
	SCA	60.1	48.5	**71.7**	0.47
	SCA-IEDP	**62.5**	61.6	63.3	0.55
SVM	SMLRAT	50.9	47.7	54	0.36
	SCA	62.1	43.5	**80.7**	0.47
	SCA-IEDP	**63.4**	**53.3**	73.5	**0.53**
DTE	SMLRAT	49.9	51.9	48	0.50
	SCA	60.4	63.2	57.6	0.58
	SCA-IEDP	**63.4**	**65.6**	**61.2**	**0.60**

4. Discussion

SCA-IEDP, as the main contribution of this paper, outperforms SCA and the compared TF and SMLRAT methods. Meanwhile, in both SCA and SCA-IEDP, we apply CP decomposition and employ spectrogram to extract time-frequency features except that in SCA-IEDP we allocate a weight to each IED according to the certainty in its labelling, SCA-IEDP performs significantly better compared to SCA in both subject-dependent and subject-independent classification approaches. SCA-IEDP is far superior, in terms of sensitivity, to SCA in detecting IEDs in both approaches. This shows that incorporating the IED probabilities in designing an IED detection model can boost its performance.

The IEDs with lower uncertainty have more impact on the learning process compared to the IEDs with higher uncertainty. Some brain activities are similar in morphology to IEDs and sometimes are recognized as IED waveform by epileptologists. In the proposed SCA-IEDP, the IEDs with higher uncertainty are given lower weights. As a result, the impact of these IEDs in the classification step decreases, leading to better performance of the model. In contrast, the proposed SCA and the compared methods do not have this particular advantage. Indeed, there has not been any method that incorporates the uncertainty in labelling the IEDs in their detection, and as far as we know, the proposed SCA-IEDP is the first approach.

The proposed models give superior performance when they are trained and tested over the same subject data (that is, subject-dependent classification approach) as compared to more generic or subject-independent classification approach. However, detecting IEDs in a subject-independent-based approach is of paramount importance. Developing a model to automatically detect the IEDs of new subjects without training on them would be worthwhile in clinical practice. Our proposed algorithms enable detection of IEDs in subject-independent-based approach, and their performance is sufficiently desirable.

Generally, none of the methods performs very well due to the fact that we use low amplitude IEDs (the scalp-visible and scalp-invisible IEDs). However, for many applications, such as seizure prediction or localization, a small improvement can be significant. Although some studies have reported higher performance but they only consider scalp-visible IEDs.[41,42] Here, iEEG has been used for scoring the IEDs. The large proportion of IEDs which can be seen in iEEG are invisible over the scalp. Our dataset includes all scalp-visible and scalp-invisible IEDs thanks to using concurrent iEEG signals for the IED annotation, causing the automatic algorithms provide poor performance.

In contrast to the TF model[19] in which the authors used only temporal and spectral IED signatures, we consider spatial IED signatures other than temporal and spectral ones. The IEDs originate from specific brain regions. Our dataset is from the patients with mesial temporal lobe epilepsy whose IEDs originate from the temporal lobe regions. Therefore, intracranial electrodes placed in the temporal lobes and, consequently, the scalp electrodes over those regions can provide more significant features. As a result, considering spatial components in designing an IED detection system can ameliorate its performance. Muti-way analysis provides an opportunity to consider spatial components and consequently boosts

the performance of an IED detection system.

In the original TF study, using the same dataset, IEDs were detected with 67% accuracy using the logistic regression classifier in the subject-dependent classification approach. Here, the TF method obtained 73% accuracy using the DTE classifier. In our TF implementation, we used a different frequency band, the IED and non-IED segment lengths, and classifiers. Apparently, these differences ameliorate the model performance.

In the referenced SMLRAT method, 95.8% accuracy has been obtained using an NB classifier. In our study, SMLRAT respectively provided the maximum accuracy of 72.9% and 50.9% in the subject-dependent and subject-independent approaches, which are significantly less than the accuracies obtained in the original paper. The main cause of this fall-off in accuracy may be due to including scalp-invisible IEDs in the classification. Here, the IEDs are annotated based on concurrent intracranial recordings, most of which are invisible over the scalp. Thus, all the scalp-visible and scalp-invisible IEDs are included in our dataset, whereas, in the referenced SMLRAT, the authors annotated the spikes using only scalp-EEG, and only scalp-visible spikes were detected. Furthermore, they detected only spikes, while our IED dataset also contains sharp waves – which are wider than spikes and sometimes similar to other brain activities. For SMLRAT, there is a huge difference in accuracy between subject-dependent and subject-independent approaches. In the subject-independent approach, we didn't introduce any new mode to the tensor (motivated by the referenced SMLRAT). In fact, the IED three-way tensors of all the subjects have been concatenated into a single four-way tensor (time, wavelet-scale, channel, and segment) in the subject-independent approach. Since the morphology and shape of IEDs can vary among subjects because of factors such as age,[43] including all IEDs along one mode of the tensor can deteriorate the decomposition performance. Therefore, SMLART gave poor performance for our dataset in the subject-independent approach. Hence, we added a new mode of subjects leading to a four-way tensor (time, channel, IED segment, and subject) for subject-independent approach, whereas we had a three-way tensor (time, channel, and IED segment) for subject-dependent approach.

The most important advantage of the proposed SCA-IEDP method is due to incorporating uncertainty levels in the IED scoring. This uncertainty can be mathematically explained by assigning lower probability values to IEDs with higher uncertainty and vice versa, making the impact of certain IEDs become more on the IED detection system.

The limitation of proposed models is that their performance in the subject-independent-based approach is not significantly high. In our dataset, the IEDs of different subjects originate from either left or right temporal region. This means the IED sources locations are different among the subjects. Since our proposed models are based on spatial components and the IED source locations are different, the performance of the proposed models decreases when a subject-independent-based approach is applied. Another cause of this fall-off in the performance of subject-independent-based approach is that the consistency of discharges decreases when all patients are pooled together. These limitations exist in SMLRAT method as well.

5. Conclusion

Developments in the identification of deep epileptiform discharges on the scalp would greatly enhance the diagnosis and management of epilepsy. Here, we propose two models, namely SCA and SCA-IEDP, for IED detection. In SCA-IEDP, as the main contribution of this work, the uncertainty in IED labeling (represented by IEDs probabilities) is incorporated in the IED detection system. We compared our proposed models with two state-of-the-art models, TF[19] and SMLRAT.[24] The IEDs are detected in two different subject-dependent and subject-independent classification approaches. In both approaches, SCA-IEDP led to the best performance. It obtained respectively the maximum accuracy of 79.9% and 63.4% in the subject-dependent and subject-independent classification approaches. Meanwhile, SMLRAT achieved respectively 72.9% and 50.9% accuracy values in the mentioned approaches. In all classifiers, TF and SMLRAT performed worse than our proposed SCA and SCA-IEDP. The obtained results show that incorporating the IED probabilities into the algorithm can ameliorate the performance of an IED detection model. Here, we used concurrent scalp-EEG and iEEG recordings. The major advantage of our work

in using this dataset is to detect the scalp-visible and scalp-invisible IEDs over the scalp. In a subject-dependent classification approach, it may not be very useful to record scalp-EEG and iEEG simultaneously and detect IEDs using scalp-EEG; whereas, in a subject-independent classification approach, it has a high impact on the diagnosis of epilepsy. That is, a subject-independent classifier can be trained using concurrent scalp and intracranial recordings of several subjects (the use of iEEG for scoring IEDs – including the scalp-visible and scalp-invisible IEDs – and the use of scalp-EEG for training the classifier). Afterward, using the trained classifier, the scalp-visible and scalp-invisible IEDs of any new subject can be detected using only scalp-EEG recordings.

However, the performances of our algorithms are not very good in subject-independent classification approach owing to different IED source locations in different subjects. As part of our future study we intend to employ a source localization algorithm and group the subjects according to their IED locations before applying a subject-independent-based approach. In addition, the use of a classification method has not been the main agenda in this work. In our future works, we may deploy more powerful classification algorithms such as neural dynamic classification algorithm,[44] dynamic ensemble learning algorithm,[45] and finite element machine classifier,[46] instead of SVM or DLDA, to boost the model performance.

Acknowledgment

We would like to thank Dr. David Martín-Lopez for his contribution to IED scoring.

Bibliography

1. U. R. Acharya, S. V. Sree, G. Swapna, R. J. Martis and J. S. Suri, Automated EEG analysis of epilepsy: a review, *Knowledge-Based Systems* **45** (2013) 147–165.
2. S. Sanei, *Adaptive Processing of Brain Signals* (John Wiley & Sons, 2013).
3. J. J. Halford, Computerized epileptiform transient detection in the scalp electroencephalogram: Obstacles to progress and the example of computerized ECG interpretation, *Clinical Neurophysiology* **120**(11) (2009) 1909–1915.
4. S. Kovac, V. N. Vakharia, C. Scott and B. Diehl, Invasive epilepsy surgery evaluation, *Seizure* **44** (2017) 125–136.
5. D. Nayak, A. Valentin, G. Alarcon, J. J. G. Seoane, F. Brunnhuber, J. Juler, C. E. Polkey and C. D. Binnie, Characteristics of scalp electrical fields associated with deep medial temporal epileptiform discharges, *Clinical Neurophysiology* **115**(6) (2004) 1423–1435.
6. M. Yamazaki, D. M. Tucker, A. Fujimoto, T. Yamazoe, T. Okanishi, T. Yokota, H. Enoki and T. Yamamoto, Comparison of dense array EEG with simultaneous intracranial EEG for interictal spike detection and localization, *Epilepsy Research* **98**(2-3) (2012) 166–173.
7. G. Alarcon, C. Guy, C. Binnie, S. Walker, R. Elwes and C. Polkey, Intracerebral propagation of interictal activity in partial epilepsy: implications for source localisation., *Journal of Neurology, Neurosurgery & Psychiatry* **57**(4) (1994) 435–449.
8. A. Ray, J. X. Tao, S. M. Hawes-Ebersole and J. S. Ebersole, Localizing value of scalp EEG spikes: a simultaneous scalp and intracranial study, *Clinical Neurophysiology* **118**(1) (2007) 69–79.
9. D. Cosandier-Rimélé, I. Merlet, J.-M. Badier, P. Chauvel and F. Wendling, The neuronal sources of EEG: modeling of simultaneous scalp and intracerebral recordings in epilepsy, *NeuroImage* **42**(1) (2008) 135–146.
10. R. Janca, P. Jezdik, R. Cmejla, M. Tomasek, G. A. Worrell, M. Stead, J. Wagenaar, J. G. Jefferys, P. Krsek, V. Komarek *et al.*, Detection of interictal epileptiform discharges using signal envelope distribution modelling: Application to epileptic and non-epileptic intracranial recordings, *Brain Topography* **28**(1) (2015) 172–183.
11. A. Antoniades, L. Spyrou, D. Martin-Lopez, A. Valentin, G. Alarcon, S. Sanei and C. C. Took, Detection of interictal discharges with convolutional neural networks using discrete ordered multichannel intracranial EEG, *IEEE Transactions on Neural Systems and Rehabilitation Engineering* **25**(12) (2017) 2285–2294.
12. L. Koessler, T. Cecchin, S. Colnat-Coulbois, J.-P. Vignal, J. Jonas, H. Vespignani, G. Ramantani and L. G. Maillard, Catching the invisible: mesial temporal source contribution to simultaneous EEG and SEEG recordings, *Brain Topography* **28**(1) (2015) 5–20.
13. K. Indiradevi, E. Elias, P. Sathidevi, S. D. Nayak and K. Radhakrishnan, A multi-level wavelet approach for automatic detection of epileptic spikes in the electroencephalogram, *Computers in Biology and Medicine* **38**(7) (2008) 805–816.
14. E. Bagheri, J. Jin, J. Dauwels, S. Cash and M. B. Westover, A fast machine learning approach to facilitate the detection of interictal epileptiform discharges in the scalp electroencephalogram, *Journal of Neuroscience Methods* **326** (2019) p. 108362.
15. H. Wieser, C. Elger and S. Stodieck, The 'foramen ovale electrode': a new recording method for the pre-

operative evaluation of patients suffering from mesiobasal temporal lobe epilepsy, *Electroencephalography and Clinical Neurophysiology* **61**(4) (1985) 314–322.
16. S. A. Sheth, J. P. Aronson, M. M. Shafi, H. W. Phillips, N. Velez-Ruiz, B. P. Walcott, C.-S. Kwon, M. K. Mian, A. R. Dykstra, A. Cole *et al.*, Utility of foramen ovale electrodes in mesial temporal lobe epilepsy, *Epilepsia* **55**(5) (2014) 713–724.
17. M. Sparkes, A. Valentin and G. Alarcon, Mechanisms involved in the conduction of anterior temporal epileptiform discharges to the scalp, *Clinical Neurophysiology* **120**(12) (2009) 2063–2070.
18. I. Karakis, N. Velez-Ruiz, J. S. Pathmanathan, S. A. Sheth, E. N. Eskandar and A. J. Cole, Foramen ovale electrodes in the evaluation of epilepsy surgery: conventional and unconventional uses, *Epilepsy & Behavior* **22**(2) (2011) 247–254.
19. L. Spyrou, D. Martín-Lopez, A. Valentín, G. Alarcón and S. Sanei, Detection of intracranial signatures of interictal epileptiform discharges from concurrent scalp EEG, *International Journal of Neural Systems* **26**(04) (2016) p. 1650016.
20. A. Antoniades, L. Spyrou, D. Martin-Lopez, A. Valentin, G. Alarcon, S. Sanei and C. C. Took, Deep neural architectures for mapping scalp to intracranial EEG, *International Journal of Neural Systems* **28**(08) (2018) p. 1850009.
21. L. Spyrou, S. Kouchaki and S. Sanei, Multiview classification and dimensionality reduction of scalp and intracranial EEG data through tensor factorisation, *Journal of Signal Processing Systems* **90**(2) (2018) 273–284.
22. A. H. Phan and A. Cichocki, Tensor decompositions for feature extraction and classification of high dimensional datasets, *Nonlinear Theory and its Applications, IEICE* **1**(1) (2010) 37–68.
23. S. Kouchaki, S. Sanei, E. L. Arbon and D.-J. Dijk, Tensor based singular spectrum analysis for automatic scoring of sleep EEG, *IEEE Transactions on Neural Systems and Rehabilitation Engineering* **23**(1) (2014) 1–9.
24. L. T. Thanh, N. T. A. Dao, N. V. Dung, N. L. Trung and K. Abed-Meraim, Multi-channel EEG epileptic spike detection by a new method of tensor decomposition, *Journal of Neural Engineering* **17** (jan 2020) p. 016023.
25. N. Kane, J. Acharya, S. Beniczky, L. Caboclo, S. Finnigan, P. W. Kaplan, H. Shibasaki, R. Pressler and M. J. van Putten, A revised glossary of terms most commonly used by clinical electroencephalographers and updated proposal for the report format of the EEG findings. Revision 2017, *Clinical Neurophysiology Practice* **2** (2017) p. 170.
26. J. J. Halford, R. J. Schalkoff, J. Zhou, S. R. Benbadis, W. O. Tatum, R. P. Turner, S. R. Sinha, N. B. Fountain, A. Arain, P. B. Pritchard *et al.*, Standardized database development for EEG epileptiform transient detection: EEGnet scoring system and machine learning analysis, *Journal of Neuroscience Methods* **212**(2) (2013) 308–316.
27. J. J. Halford, M. B. Westover, S. M. LaRoche, M. P. Macken, E. Kutluay, J. C. Edwards, L. Bonilha, G. P. Kalamangalam, K. Ding, J. L. Hopp *et al.*, Interictal epileptiform discharge detection in EEG in different practice settings, *Journal of Clinical Neurophysiology* **35**(5) (2018) p. 375.
28. J. J. Halford, A. Arain, G. P. Kalamangalam, S. M. LaRoche, B. Leonardo, M. Basha, N. J. Azar, E. Kutluay, G. U. Martz, W. J. Bethany *et al.*, Characteristics of EEG interpreters associated with higher interrater agreement, *Journal of Clinical Neurophysiology* **34**(2) (2017) p. 168.
29. E. Acar, D. M. Dunlavy and T. G. Kolda, A scalable optimization approach for fitting canonical tensor decompositions, *Journal of Chemometrics* **25**(2) (2011) 67–86.
30. E. Acar, D. M. Dunlavy, T. G. Kolda and M. Mørup, Scalable tensor factorizations for incomplete data, *Chemometrics and Intelligent Laboratory Systems* **106**(1) (2011) 41–56.
31. T. G. Kolda and B. W. Bader, Tensor decompositions and applications, *SIAM Review* **51**(3) (2009) 455–500.
32. T. G. Kolda, Multilinear operators for higher-order decompositions., tech. report, Sandia National Laboratories (2006).
33. R. Harshman, Foundations of the parafac procedure: Models and conditions for an" explanatory" multimodal factor analysis, *UCLA Working Papers in Phonetics* (1970).
34. S. Haykin, *Neural networks and learning machines.* (New York: Prentice Hall,, 2009).
35. O. Faust, U. R. Acharya, H. Adeli and A. Adeli, Wavelet-based EEG processing for computer-aided seizure detection and epilepsy diagnosis, *Seizure* **26** (2015) 56–64.
36. H. Adeli, Z. Zhou and N. Dadmehr, Analysis of EEG records in an epileptic patient using wavelet transform, *Journal of Neuroscience Methods* **123**(1) (2003) 69–87.
37. U. R. Acharya, Y. Hagiwara and H. Adeli, Automated seizure prediction, *Epilepsy & Behavior* **88** (2018) 251–261.
38. P. W. Mirowski, Y. LeCun, D. Madhavan and R. Kuzniecky, Comparing SVM and convolutional networks for epileptic seizure prediction from intracranial EEG, *2008 IEEE Workshop on Machine Learning for Signal Processing*, IEEE2008, pp. 244–249.
39. S. Sun, C. Zhang and D. Zhang, An experimental evaluation of ensemble methods for EEG signal classification, *Pattern Recognition Letters* **28**(15) (2007) 2157–2163.
40. J. R. Quinlan, Bagging, boosting, and c4. 5, *AAAI/IAAI, Vol. 1*, 1996, pp. 725–730.
41. F. I. Argoud, F. M. De Azevedo, J. M. Neto and

E. Grillo, SADE: An effective system for automated detection of epileptiform events in long-term EEG based on context information, *Medical and Biological Engineering and Computing* **44**(6) (2006) 459–470.
42. J. Thomas, J. Jin, P. Thangavel, E. Bagheri, R. Yuvaraj, J. Dauwels, R. Rathakrishnan, J. J. Halford, S. S. Cash and B. Westover, Automated detection of interictal epileptiform discharges from scalp electroencephalograms by convolutional neural networks, *International journal of neural systems* **30** (November 2020) p. 2050030.
43. E. Aanestad, N. E. Gilhus and J. Brogger, Interictal epileptiform discharges vary across age groups, *Clinical Neurophysiology* **131**(1) (2020) 25–33.
44. M. H. Rafiei and H. Adeli, A new neural dynamic classification algorithm, *IEEE Transactions on Neural networks and Learning Systems* **28**(12) (2017) 3074–3083.
45. K. M. R. Alam, N. Siddique and H. Adeli, A dynamic ensemble learning algorithm for neural networks, *Neural Computing and Applications* **32**(12) (2020) 8675–8690.
46. D. R. Pereira, M. A. Piteri, A. N. Souza, J. P. Papa and H. Adeli, Fema: a finite element machine for fast learning, *Neural Computing and Applications* **32**(10) (2020) 6393–6404.